Co-registered Hyperspectral and Stereo Image Seafloor Mapping from an Autonomous Underwater Vehicle

Daniel L. Bongiorno
Defence Science & Technology Group
Australian Centre for Field Robotics
University of Sydney
daniel.bongiorno@dsto.defence.gov.au

Mitch Bryson
Australian Centre for Field Robotics
University of Sydney
m.bryson@acfr.usyd.edu.au

Tom C. L. Bridge
ARC Centre of Excellence for Coral Reef Studies
James Cook University
thomas.bridge@jcu.edu.au

Donald G. Dansereau
ARC Centre of Excellence for Robotic Vision
Queensland University of Technology
donald.dansereau@qut.edu.au

Stefan B. Williams
Australian Centre for Field Robotics
University of Sydney
s.williams@acfr.usyd.edu.au

Abstract

We present a new method for in-situ high resolution hyperspectral mapping of the seafloor utilising a spectrometer co-located and co-registered with a high resolution colour stereo camera system onboard an Autonomous Underwater Vehicle (AUV). Hyperspectral imagery data has been used extensively for mapping and distinguishing marine seafloor habitats and organisms from above-water platforms (such as satellites and aircraft), but at low spatial resolutions and at shallow water depths (<10m). The use of hyperspectral sensing from in-water platforms (such as AUVs) has the potential to provide valuable habitat data in deeper waters and with high spatial resolution. Challenges faced by in-water hyperspectral imaging include difficulties in correcting for water column effects and the spatial registration of point/line-scan hyperspectral sensor measurements. The methods developed in this paper overcome these issues through co-registration with a high spatial resolution, stereo colour camera and precise modelling and compensation of the water column properties that attenuate hyperspectral signals. We integrated two spectrometers into our SeaBED class AUV, and one on-board a support surface vessel to measure and estimate the effects of light passing through the water column. Spatial calibration of the spectrometers/stereo cameras and the synchronized acquisition of both sensors allowed for spatial registration of the resulting hyperspectral reflectance profiles. We demonstrate resulting hyperspectral imagery maps with a spatial resolution of 30cm over large areas of the seafloor that are not adversely effected by above-water conditions (such as cloud cover) that would typically prevent the use of remote-sensing methods. Results are presented from an AUV mapping survey of a coral reef ecosystem over Pakhoi Bank on the Great Barrier Reef, Queensland, Australia demonstrating the ability to reconstruct hyperspectral reflectance profiles for a diverse range of abiotic and biotic coverage types including sand, corals, seagrass and algae. Profiles are then used to automatically classify different coverage types with a 10-fold cross validation accuracy of 91.99% using a linear Support Vector Machine (SVM).

1 Introduction

The ocean floor contains a multitude of different habitats that harbour and support marine life and ecosystems such as coral reefs, kelp forests and seagrass meadows, which possess immense social and economic value and are expected to suffer increasing environmental pressures in the coming years and decades (Hoegh-Guldberg et al., 2007) (Wilkinson, 2008). Conservation and management strategies used to monitor these habitats rely on regularly updated data on their structure, composition and health, which are acquired and interpreted from a range of sources including remote sensing (satellite and aircraft imaging from above the water (Andréfouët et al., 2002)) and in-situ/underwater means (such as visual observations by divers, ship-towed video data and imagery from underwater robotic platforms such as Autonomous Underwater Vehicles (AUVs) (Williams et al., 2010)). Remote sensing from platforms such as satellites and airborne vehicles provide broad-scale information on seafloor habitats but at low spatial resolutions (>2.4m per pixel (Wang et al., 2010)) and are limited to imaging the ocean floor in water depths no greater than 20m (Kobryn et al., 2013). These platforms make up for their lack of spatial resolution by using sophisticated multi-spectral and hyperspectral imaging systems that provide images with tens to hundreds of precise colour channels (Mishra et al., 2007) and have been exploited to classify seafloor substrates (Idris et al., 2009; Hochberg and Atkinson, 2003; Guild et al., 2003) and biological communities (Holden and LeDrew, 2001; Volent et al., 2007). In contrast, in-situ underwater imaging systems such as towed video and AUVs provide data with very high spatial resolutions (sub-centimeter per pixel, depending on operating altitude) but over relatively smaller extents (constrained by vehicle range and operating altitude). These platforms typically deploy only monochrome or three-colour imagery (red-green-blue) (Williams et al., 2012; Campos et al., 2015), owing to the difficulties of fielding hyperspectral imaging systems used by satellites and aircraft in the water and the mitigation of the effects of water attenuation and scattering on light from a moving platform.

In this paper we present a novel underwater imaging system and series of calibration and post-processing procedures designed to derive *hyperspectral* imagery maps of the seafloor using an AUV, thus combining the advantages of both in-situ and remote sensing sources of data for monitoring marine habitats. Instead of deploying a large, heavy and potentially expensive hyperspectral *imaging* system (i.e. a sensor that contains either a 1D or 2D array of sensing elements that measure incoming light at different spectra/colours), our system utilises a single-point hyperspectral radiometer co-mounted with a three-colour stereo camera that relies on the forward motion of the AUV (and a precise series of processing steps to spatially register spot measurement on the seafloor) to build up a hyperspectral image. The resulting sensor combination is light-weight, relatively in-expensive (compared to hyperspectral imagers) and provides higher spectral resolution and better signal to noise performance than a hyperspectral imaging sensor. We develop a processing methodology that reconstructs the hyperspectral reflectance (ratio of out-going to incoming light across many spectra/colours) of the seafloor by accounting for ambient light conditions, lights from strobes on-board the AUV and the Inherent Optical Properties (IOPs) of the surrounding water column which cause attenuation of light underwater at different wavelengths which must be corrected for. We demonstrate the ability to reconstruct hyperspectral reflectance profiles from a moving AUV platform for a diverse range of abiotic and biotic coverage types including sand, corals, seagrass and algae and further develop automatic seafloor classification algorithms using hyperspectral signatures and supervised machine learning methods. Results of the system are presented using data collected by the Sirius AUV over coral reef habitats at Pakoi Bank on the Great Barrier Reef, Australia.

1.1 Related Work

Imaging the seafloor from above or within the water column provides a number of challenges. The air-water interface acts to refract and reflect away light depending on wind and wave conditions, limiting the spatial resolution and clarity with which measurements can be made from above the water (Mobley, 1994). When imaging is performed from within the water (e.g. using an AUV), wavelength-selective attenuation and scattering of light results in loss of image clarity with distance to the object and a shift in the apparent object colour (Mobley, 1994). Various approaches have been used to account for colour variations in underwater imagery including active illumination (Vasilescu et al., 2010), qualitative machine learning (Torres-Mendez

and Dudek, 2005) and image formation model-based approaches (Bryson et al., 2015). Object and organism colour has been cited as an important feature for classification, identification and measurement (Mehta et al., 2007) however limitations in the ability to accurately reconstruct colour in previous work has resulted in limited use (Clement et al., 2005) (Pizarro et al., 2008). Instead most approaches use spatial texture-based features (Clement et al., 2005) (Beijbom et al., 2012) as the primary means of organism classification in images. In contrast, organism colour (measured at hyperspectral resolutions) has been used extensively in field-based spectroscopy studies where data from point-based sensors has been used to distinguish coral genera (Roelfsema and Phinn, 2012) and examine coral health (Holden and LeDrew, 2001). Measurements in these studies are made manually by divers by placing the sensor very close (<10cm) from the target surface, thus avoiding the issue of water column influence, but limiting the extent over which measurements can be made to a handful of point-based samples.

The use of hyperspectral measurements over broader extents made from within the water is limited. (Johnsen et al., 2013) discusses an underwater sliding hyperspectral camera test rig, however results are limited to a static, non-moving platform. Hyperspectral radiometers (or spectrometers) have been used on AUVs to measure properties of the water column itself (Hartmann et al., 2009; English and Carder, 2006) and also to measure the seafloor reflectivity (English and Carder, 2006), but at limited, single point samples. Previous studies have not demonstrated the capacity to produce spectral reflectance measurements at a fine spatial resolution and over a broad extent nor measurements that have been corrected for the influence of the water column. The ability to recover in-water hyperspectral reflectance measurements over marine habitats such as coral reefs has the potential to provide a valuable source of data to complement existing approaches to habitat classification and assessment based on automatic machine learning methods currently deployed on monochrome and three-colour images collected by AUVs (Friedman et al., 2011).

1.2 Contribution of our work

In this work we are concerned with the ability to create geo-referenced maps of hyperspectral reflectance of the seafloor that can be used on their own (or with additional high-resolution stereo imagery) to automatically identify and classify seafloor organisms and habitat types, using data collected from a moving robotic platform (an AUV). We build upon previous developments in hyperspectral imaging, image-based data fusion and classification to develop a system of AUV data collection and processing to achieve this aim. The key contributions of this work are to

1. develop a novel system by which measurements from a spectrometer can be georeferenced and mapped to the seafloor from a moving AUV.

2. develop a system of data collection and processing that allows for the recovery of hyperspectral reflectance of the seafloor by modelling and measurement of the effects and interactions of water column attenuation, on-board lighting, ambient lighting and the air-water interface.

Additionally, our system is demonstrated to effectively distinguish between different seafloor biota through the development of automatic classification algorithms based on hyperspectral reflectance profiles, with results presented over a broad-scale AUV mission. In contrast to previous work in underwater field spectroscopy (Roelfsema and Phinn, 2012) (Holden and LeDrew, 2001), we develop a method for measuring tens of thousands of individual reflectance profiles over kilometres of the seafloor through the use of an AUV and account of the effects of the water column on underwater light. In contrast to past work on underwater colour correction using three-colour images (Vasilescu et al., 2010) (Torres-Mendez and Dudek, 2005)(Bryson et al., 2015), we employ a light attenuation model-based technique to correct colour at *hyperspectral* resolutions and use this data to effectively classify seafloor substrates and organisms.

2 Methodology

2.1 Overview of approach

A flow chart of our data collection and data processing method is shown in Figure 1. The system utilizes multiple, sychronised spectrometer measurements above and below the surface of the water to measure and compensate for the effects of ambient and artificial lighting sources required to measure the reflectance of light at the seafloor. A model of the air-water interface is derived from measurements taken from the ship-borne inertial measurement unit (IMU), GPS position of the ship, time of day, conductivity and temperature of the water, and wind data for the region. Ambient light passing from the surface of the water to the AUV is measured by an upwards-looking spectrometer mounted to the AUV. Data from these two sensors is incorporated to effectively measure the contribution of ambient light at the seafloor surface (differences in intensity across the visual spectrum) and estimate inherent optical properties of the water. Reflected light from the seafloor is measured by a downwards-looking spectrometer on the AUV and processed in conjunction with this information to estimate the reflectance of the seafloor. Reflectance measurements are spatially geo-registered via information derived by the stereo camera system, which also provides relative range information to the seafloor surface which is necessary to quantify and compensate the effects of the water column on the downwards-looking spectrometer measurements. The resulting geo-referenced spectral profiles are then used to classify seafloor biota using a supervised learning framework based on a small number of training examples provided by a marine biologist from the associated colour stereo camera images.

2.2 Autonomous Underwater Vehicle

The *Australian Centre for Field Robotics (ACFR), University of Sydney* operates a Woods Hole Oceanographic Institution (WHOI) Seabed class AUV (Singh et al., 2004), the SIRIUS, (see Figure 2b) that carries a suite on on-board sensors including navigation sensors (Doppler Velocity Log (DVL), Ultra Short Base Line (USBL) acoustic positioning system, GPS receiver, depth and attitude sensors), water sensors (CDOM, Chlorophyll, backscatter) and seafloor sensors (multibean sonar and stereo camera system with LED strobes for artificial lighting) (Williams et al., 2010). The AUV typically travels at 0.5m/s and aims to maintain an altitude of 2m from the seabed. Data from the stereo camera and other navigation sensors is post-processed to produce 3D topographic and colour imagery mosaics using techniques in Simultaneous Localisation And Mapping (SLAM), structure-from-motion and terrain reconstruction (see (Williams et al., 2012) for details).

2.3 Spectrometer data collection and calibration

For our proposed system, a series of spectrometers were installed aboard the AUV SIRIUS and on the support surface vessel (a 35m long research vessel operating in the vicinity of the AUV). Figure 1 shows the positioning of these spectrometers. The two upward looking spectrometers were used to collect downwelling irradiance on the surface before the light enters the water (from the surface-based support vessel) and as the surface light (sunlight and skylight) passes the vehicle (mounted to the AUV). A downwards facing spectrometer is co-located with the stereo camera and used to collect the spectra of the imaged seabed. Figure 2a shows a photo of the window of the camera housing showing the positioning of the spectrometer co-located with the stereo cameras. The stereo cameras have been radiometrically characterised using the method from (Bongiorno et al., 2013a).

2.3.1 AUV downward facing spectrometer

To implement our method of spectral imaging onboard SIRIUS we re-engineered the stereo camera housing to fit an Ocean Optics USB 2000+ spectrometer (dimensions: 89.1mm x 63.3mm x 34.4mm). The USB 2000+ collects 2048 spectral bins with a Full Width at Half Maximum (FWHM) of 7.7nm it is sensitive in the spectral region of 340nm - 1032nm. The spectrometers optical entrance was connected via a 10cm fibre optic cable

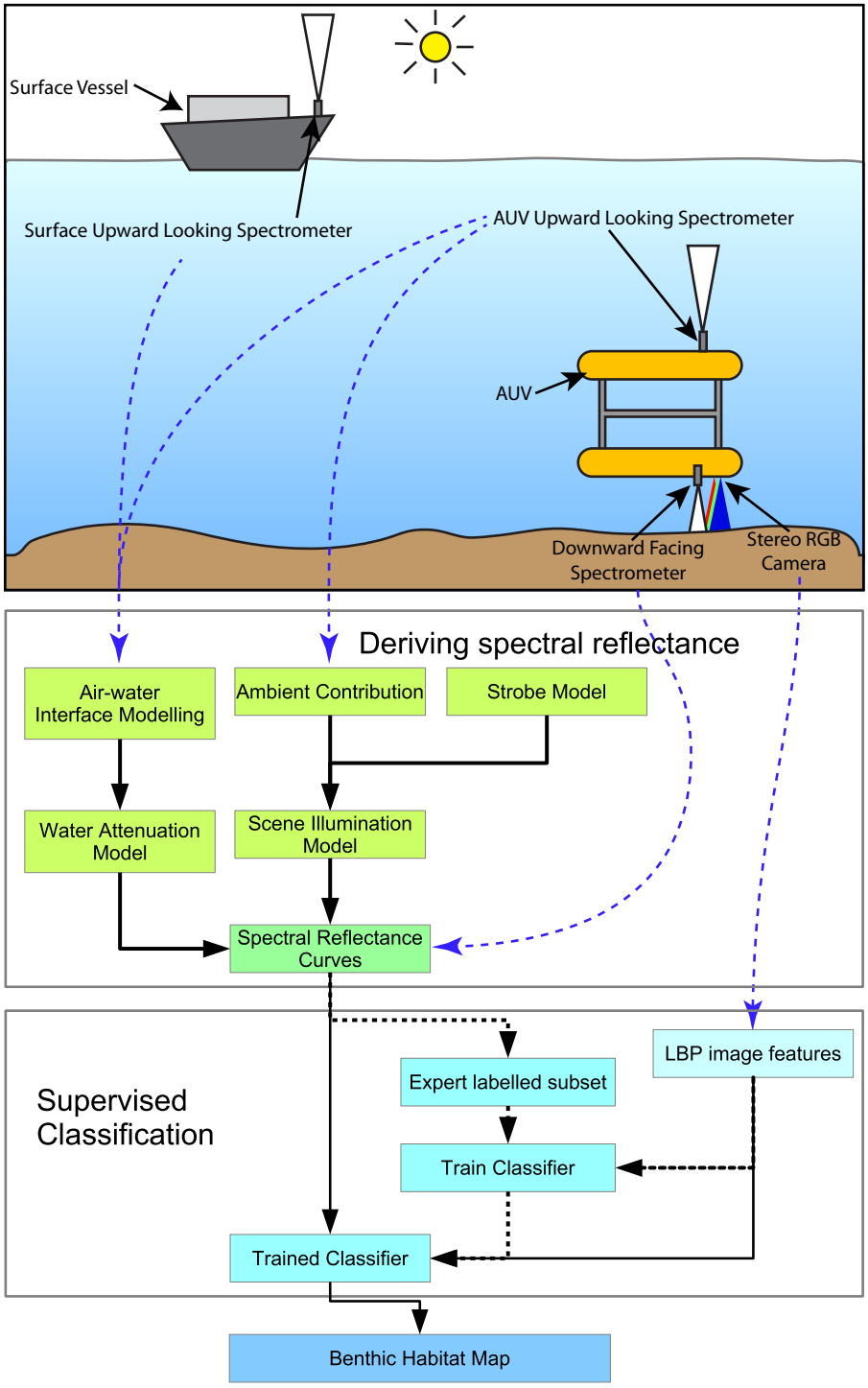

Figure 1: The first Stage of the processing is data acquisition from the ship and Autonomous Underwater Vehicle (AUV) borne sensors (these include upward facing spectrometers on the AUV and surface vessel, downward facing spectrometer, stereo camera, IMU on the surface vessel, conductivity and temperature sensor). The second stage involves the generation the water, air/water interface and illumination models which derive the spectral reflectance curves. The classifier is trained by an expert labelled subset of the data, which then generates a seafloor habitat map.

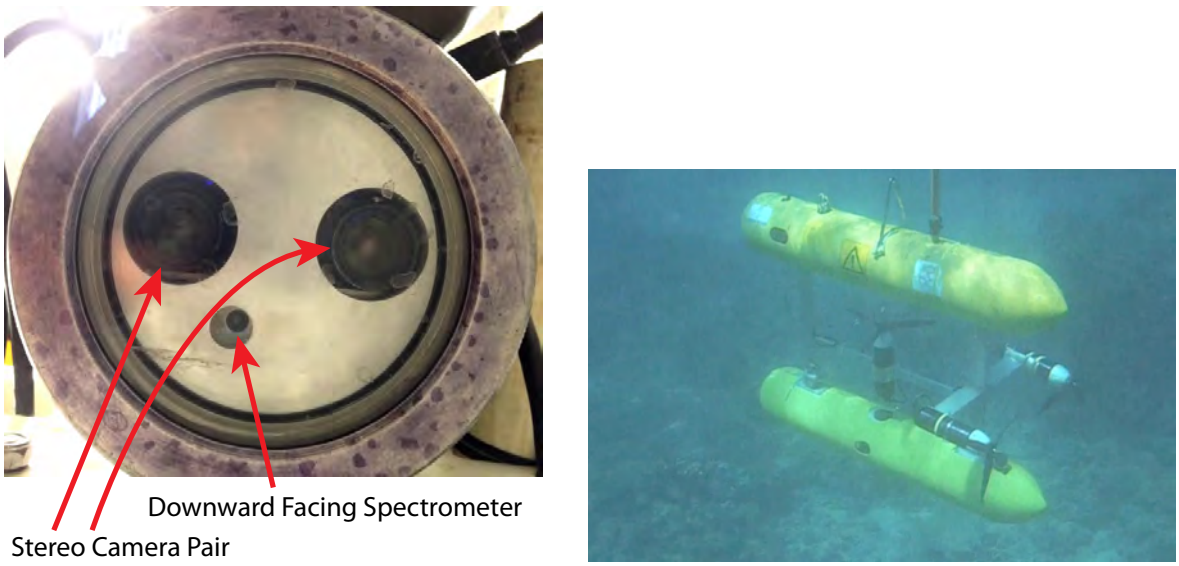

(a) (b)

Figure 2: (2a): A view of the camera housing window showing the positioning of the spectrometer's aperture (small hole) with respect to the lenses of the stereo cameras (two larger holes). The downward facing spectrometer used was an Ocean Optics USB 2000+ with a wavelength range of 340nm - 1032nm, and a FWHM of 7.7nm. (2b): Sirius AUV underwater.

to a collimating lens[1] co-located with the stereo camera lenses at the window of the camera system (Figure 2a). The collimating lens allowed for the focusing of the Field-of-View (FOV) of the spectrometer to a sharp edged spot. Measurement acquisition from the spectrometer was synchronized to the image acquisition by the stereo cameras and firing of the strobes through a common trigger signal. An auto-exposure algorithm was implemented to adjust the spectrometer exposure/integration time to achieve a desired mean signal strength using measured signals over the previous 30 second interval. In practice, only wavelengths in the range 400 to 800nm were used in subsequent processing, owing to the almost complete absorption of light of wavelengths outside this range while in the water. A Savitzky-Golay filter (Savitzky and Golay, 1964) was used to reduce noise in the measured spectra. The window of the underwater housing in front of the spectrometer lens was made of acrylic and laboratory tests prior to AUV deployment confirmed that this material provided consistent transmission across wavelengths of 400 to 800nm.

2.3.2 AUV upward looking spectrometer

For collecting the downwelling irradiance through the water column above the AUV, an AUV-mounted, upwards looking spectrometer was installed on the top of the AUV. This spectrometer samples the sun and sky light penetrating down through the water column from the surface above. The spectrometer used was a low-cost microspectrometer (Ocean Optics STS-200 VIS), chosen based on its high resolution and small form factor (40mm x 42mm x 24mm) with a spectral range of 335nm to 820nm. A cosine corrector[2] was installed on the fore-optics, for integrating the incoming radiance. The spectrometer operated in a different underwater housing to the downward facing spectrometer and stereo camera system; all sensor data was logged to a network sychronised timestamp at a rate of 1Hz. Synchronisation of the data between this spectrometer and the other sensors achieved via post-processing.

[1] Ocean Optics 74-VIS: 350-2000nm wavelength range, f/2 BK-7 glass
[2] Ocean Optics CC-3: Opaline glass, 180° FOV, 350-1000nm wavelength range

2.3.3 Ship-borne upward looking spectrometer

To measure the irradiance before it enters the water, an upwards looking spectrometer was installed on the support vessel on the surface. This spectrometer is mounted in the zenith position in an unobstructed high vantage point on the ship. The sensor is identical to the upward facing spectrometer on the AUV (Ocean Optics STS-200 VIS), with the same fore-optics (cosine corrector) and was mounted inside a waterproof housing with an acrylic window. The spectral data was logged to a ship-based computer over RS-232 serial using a custom Python-based driver. An auto-gain system was implemented in the device driver similar to the one on the downward looking spectrometer (see Section 2.3.1). The time on the surface data logging computer was synchronised with the AUV's onboard computer preceding each dive. The data acquisition system logged spectra at approximately 1Hz. Position, roll, pitch and heading was recorded from an IMU mounted on the support vessel sampled at 10Hz, and later used to to process the fraction of light entering the water from directly above. A Savitzky-Golay filter (Savitzky and Golay, 1964) was used to reduce noise in the measured spectra from both the ship-borne and AUV-mounted, upwards looking spectrometers.

2.3.4 Relative radiometric calibration of spectrometers

Each of the spectrometers used were sensitive to slightly different wavelengths of light, based on differences in the units themselves, collimating lenses and materials in the underwater housing; a relative radiometric calibration procedure was performed to provide a wavelength-dependent scaling factor for each spectrometer such that radiance measurements were consist amongst the three units. The scaling factor was determined by imaging of a common white calibration panel prior to AUV deployment.

2.4 Spatial calibration of downwards-looking spectrometer and stereo camera system

We used an existing procedure (Bongiorno et al., 2013b) to spatially co-register the footprint of both the downwards looking spectrometer and stereo camera system, performed prior to AUV operations. The collimating optics used at the front of the downwards looking spectrometer resulted in a focused footprint of the sensor on the target surface; this footprint has an intrinsic spatial distribution of sensitivity within the field of view which is not necessarily circular and uniform. Additionally, the optical axis of the spectrometer is not aligned to the optical axis of the camera. A two-stage calibration procedure was developed to account for these effects.

The first stage of the calibration involved estimation of the spectrometer field of view and spatial sensitivity distribution within the field of view of the stereo camera image. The method used a laboratory setup in a dark room in which both sensors were pointed towards a computer monitor that produced a small white square against a black field. The position of the white square was varied across a regular pattern and the resulting position of the square and spectrometer-measured intensity recorded. The resulting intensities were used to produce a map of spectrometer sensitivity as a function of image position.

The second stage of the calibration involved computing a relative translation and rotation value between the optical centers of the camera and spectrometer by repeating the imaging of the monitor and varying distances from the camera. The resulting calibration procedure produced a relationship that described the field of view of the spectrometer footprint within the camera image space as a function of the range to the target.

When operating on the AUV, the calibration relationship was used to project the position of spectrometer readings into the camera space based on information about the range to targets provided by the stereo-imaging system.

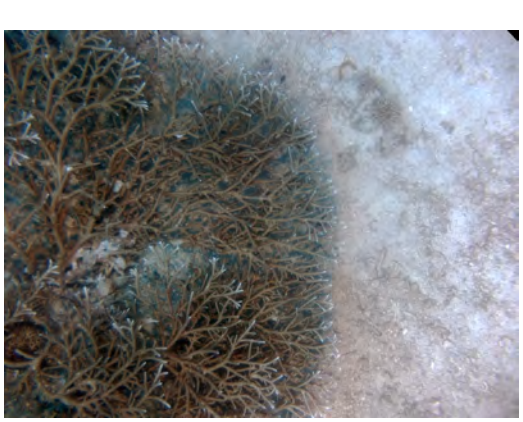

(a) Colour image from stereo camera

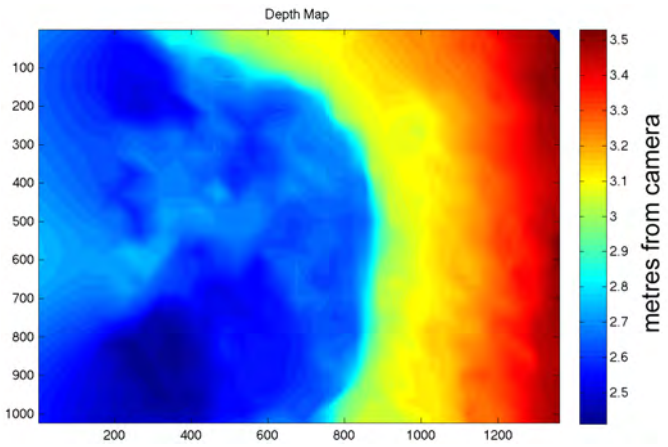

(b) Depth map

Figure 3: An example of a depth map derived from the 3D mesh generated from the stereo camera data, this is generated from the 3D mesh created from the stereo camera data. These depth maps allow for an accurate measurement of altitude for the spectrometer reading. An accurate altitude reading is critical for correcting the spectra for water attenuation.

2.5 Water column modeling and reflectance reconstruction

This section describes our methodology for recovering measurements of hyperspectral reflectance from the seafloor using spectrometer data acquired by the different spectrometers. Hyperspectral reflectance of surfaces on the seafloor is defined as the ratio of radiance of light leaving the surface to the incident light arriving at the surface, as a function of different light wavelengths. To estimate these two radiance values information is required on the light leaving the surface (measured by the downwards looking spectrometer) and light available in the scene from both the artificial strobes carried on the AUV and the ambient light available from the sun (measured by the support vessel spectrometer). Information is also required on the wavelength-dependant attenuation of these different light sources as they move through the water column.

2.5.1 Water column modelling

The molecules of a body of water absorb light in a wavelength-dependant manner, depending on the distance travelled through the water via Lambert-Beers law:

$$E_d(\lambda) = E_s(\lambda)e^{-K(\lambda)d} \tag{1}$$

where $E_d(\lambda)$ is the irradiance with respect to wavelength λ at distance d, $E_s(\lambda)$ is the irradiance at zero distance, $K(\lambda)$ is the diffuse downwelling attenuation coefficient for the water (a function of wavelength). Estimates of the diffuse downwelling attenuation coefficient $K(\lambda)$ can be ascertained by measuring the ratio of irradiance before and after travelling through a known distance of water by rearranging Equation 1:

$$K(\lambda) = -\frac{1}{d}\log_e\left(\frac{E_s(\lambda)}{E_d(\lambda)}\right) \tag{2}$$

Synchronized measurement of hyperspectral radiance from both the surface-based and AUV-mounted upwards looking spectrometers were used to estimate the attenuation coefficient of the water column in which the AUV operated. Measurements from the surface-based spectrometer were processed to account for the

motion of the vessel and the effect of the air-water interface (see next subsection) to estimate the radiance of light entering the water column above the AUV. This value was then combined with the upwards looking spectrometer measurements via Equation 1 to estimate the attenuation coefficient of the water column. Estimates of the coefficient were made for each measurement to account for variations encountered when moving from one location to the next by the AUV (differencing in water attenuation properties induced by changes in, for example, water temperature, salinity, constitutes etc.).

2.5.2 Compensation of air-water interface effects

The complex nature of the air-water interface results in changes in the intensity of light just above and just below the water's surface depending on the time of day, wind speed and other water properties. Light passing through the air-water interface will be reduced through various factors such as reflection and refraction, arising from the angle of the sun, waves and wind elements. A series of processing steps were used to derive estimates of the light radiance just under the water surface from measurement above the surface.

To determine the amount of reflection from the interface, the refractive index is derived using the empirical equation for the index of refraction of seawater Equation (3) (Quan and Fry, 1995) which is a function of wavelength (λ in nm), salinity (S) and temperature (T).

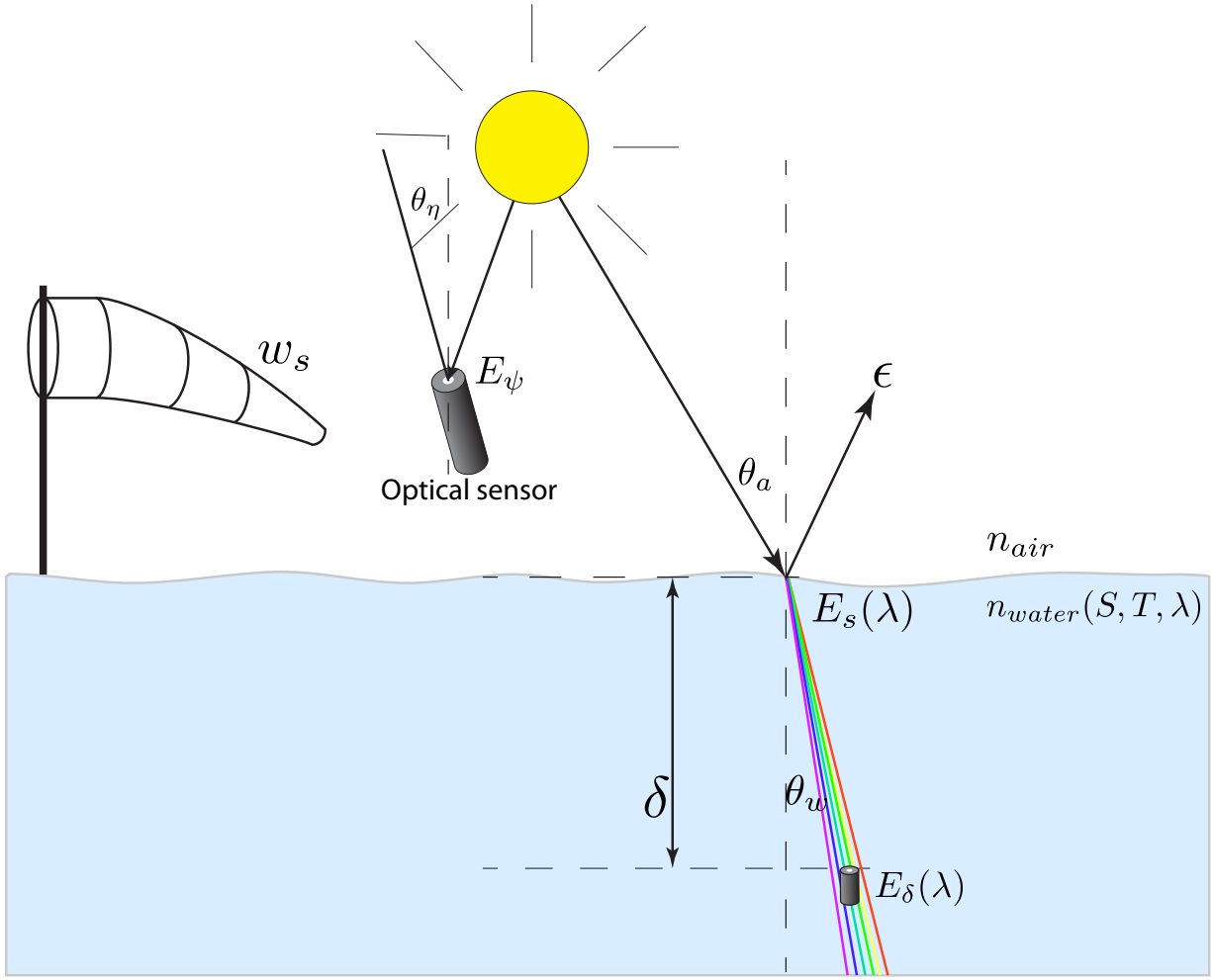

Figure 4: This shows the complete parameters obtained for modelling for the air-water interface.

$$n(S,T,\lambda) = n_0 + (n_1 + n_2 T + n_3 T^2)S + n_4 T^2 + \frac{n_5 + n_6 S + n_7 T}{\lambda} + \frac{n_8}{\lambda^2} + \frac{n_9}{\lambda^3} \tag{3}$$

$n_0 = 1.31405$ $n_1 = 1.779 \times 10^{-4}$ $n_2 = -1.05 \times 10^{-6}$ $n_3 = 1.6 \times 10^{-8}$
$n_4 = -2.02 \times 10^{-6}$ $n_5 = 15.868$ $n_6 = 0.01155$ $n_7 = -0.00423$
$n_8 = -4382$ $n_9 = 1.1455 \times 10^6$

From the derived refractive index $n_{water}(S,T,\lambda)$, Snell's Law Equation (4) was used to determine the exit angle of the light in the water:

$$\theta_w(\lambda) = \arcsin\left(\frac{n_{air}}{n_{water}(S,T,\lambda)}\sin(\theta_a(\lambda))\right) \tag{4}$$

Where the index of refraction of air $n_{air} \approx 1$ and the entry angle ($\theta_a(\lambda)$) is the zenith angle of the sun. The refracted angle at which the light now passes through the water after the air-water interface is defined by $\theta_w(\lambda)$. A proportion of light will be reflected at the interface surface and does not pass into the water. The reflectance r at the surface is a function of the zenith angle of the incident light in air (θ_a) and the exit angle (relative to vertical) in water θ_w. This relationship is given by Fresnel's Equation:

$$r = \frac{1}{2}\frac{\sin^2(\theta_a - \theta_w)}{\sin^2(\theta_a + \theta_w)} + \frac{1}{2}\frac{\tan^2(\theta_a - \theta_w)}{\tan^2(\theta_a + \theta_w)} \tag{5}$$

There will also be light reflection from wind derived white caps on the surface of the water which can be modeled using a white cap percentage (Spillane et al., 1986):

$$whitecap\% = 2.692 \times 10^{-5} w_s^{2.625} \tag{6}$$

where windspeed w_s is in metres per second, and was obtained from an Australian Institute of Marine Science (AIMS) offshore weather station at Davies Reef ($18.83S, 147.63E$) which was close to our mapping sites. The work of Koepke *et al.* (Koepke, 1984) found the white caps had an effective reflectance of 22% over time due to their short life. The extinction percentage (ϵ) of the irradiance passing through the air-water interface is derived in Equation (7) with the resultant light irradiance just below the surface E_s being defined in Equation (8).

$$\epsilon = whitecap\% \times 22\% + r \tag{7}$$

Finally, correction was applied for the changes in the zenith angle of the measuring spectrometer above the water, owing to the roll and pitch of the surface vessel, which were recorded using an IMU and GPS navigation system, with time-synchronized measurements to the spectrometer. The resulting irradiance of light just below the surface of the water ($E_s(\lambda)$) is computed using Equation (8):

$$E_s(\lambda) = E_\psi(\lambda)\left(\frac{1-\epsilon}{\cos(\theta_\eta)}\right) \tag{8}$$

where θ_η is the angle between the sensor's optical axis and the zenith angle at the time of acquisition and $E_\psi(\lambda)$ is the irradiance measurement from the above water optical sensor. Measurements of $E_s(\lambda)$ are combined with measurements from the AUV-mounted upwards looking spectrometer $E_s(\lambda)$ and the depth of the AUV (calculated from the depth sensor on-board the AUV) to estimate $K(\lambda)$ using Equation 2.

2.5.3 Modelling of illuminating light sources

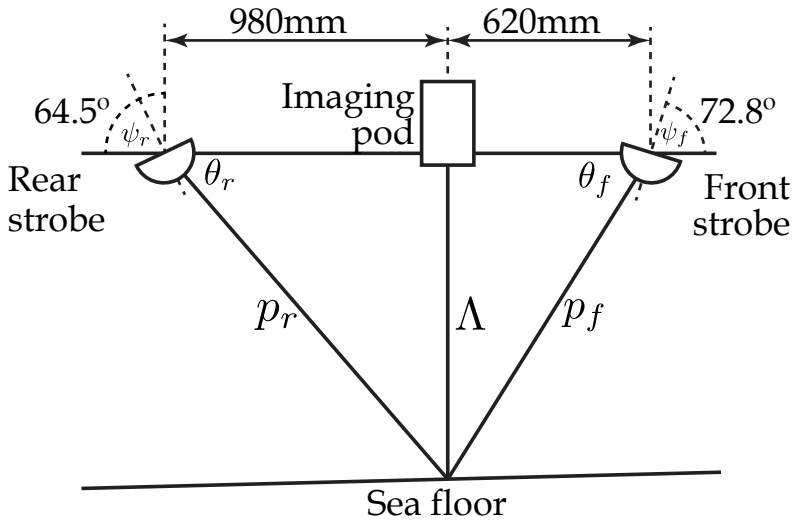

Figure 5: This shows the layout of the imaging pod and the strobes on our AUV. This is important for modelling the strobe illumination: Λ - altitude of vehicle & imaging pod, p_f & p_r - strobe path length from strobe to scene for front and rear strobes respectively, θ_f & θ_r - illumination angle as a function of altitude and linear offset on the AUV, ψ_f & ψ_r - fixed tilt of the strobes on the vehicle.

Light arriving at the seafloor which is then reflected and measured by the AUV is a result of a combination of the ambient light (from the sun) and on-board strobes. In this section we discuss models used to calculate the total irradiance of light arriving at the surface (where the AUV is imaging) from these two sources. Figure 5 illustrates the physical layout of the front and rear mounted strobes on the AUV, the imaging pod and path lengths of light to the observed location of the seafloor used in the modelling.

The spectral irradiance of the strobes was measured using both an in-air and in-water procedure. Spectral measurements of light from the strobes reflected against a white calibration target (Spectralon panel) were measured in air in dark surroundings (so as to isolate light from the strobe), in which losses through the atmosphere were assumed negligible. Additionally an in water procedure was used in which a white object was measured from the spectrometer with both strobes on and strobes off. The strobe spectral power was estimated by subtracting the strobe-off measurement from the strobe-on measurement and accounting for the attenuation of water, calculated using Equation 2 and using additional upwards looking measurement at the AUV depth and from the surface. The resulting spectra of both procedures agreed.

The irradiance of light arriving at the seafloor surface from each strobe is a function of both the distance and relative pointing angle of the strobe, which varied depending on the altitude of the AUV above the seafloor. The point spread of light from each strobe's direction vector was estimated using a cosine drop-off relationship such that the total power of light leaving each strobe, in the direction of the imaged section of seafloor (E_f and E_r, front and rear strobes) was:

$$E_f = \cos(|\theta_f - \psi_f|) \tag{9}$$

$$E_r = \cos(|\theta_r - \psi_r|) \tag{10}$$

where θ_f, θ_f, ψ_r and ψ_r are the angles illustrated in Figure 5. Light from the strobes is then attenuated through a length of water column p_f and p_r. In addition there is a contribution from the ambient light (from the sun), these are combined in Equation 11 to compute the total irradiance of light arriving at the seafloor surface ($E_{seafloor}(\lambda)$):

$$E_{seafloor}(\lambda) = E_f(\lambda)e^{(-K(\lambda)p_f} + E_r(\lambda)e^{(-K(\lambda)p_r} + E_d(\lambda)e^{(-K(\lambda)\Lambda)} \tag{11}$$

where information on the relative position of the imaged section of seafloor and hence distances Λ, p_f and p_r were all provided by the navigation estimates and 3D terrain surface models computed by the AUV (see Section 2.2).

2.5.4 Calculation of seafloor reflectance

Final estimates of the seafloor reflectance were obtained through the ratio of estimated light arriving at the surface and measured light leaving the surface:

$$R(\lambda) = \frac{E_u(\lambda)}{E_{seafloor}(\lambda)} \tag{12}$$

where $E_u(\lambda)$ is the light leaving the seafloor surface and was calculated from the downwards looking spectrometer measurements by accounting for the attenuation during the path up to the imaging pod using:

$$E_u(\lambda) = \frac{1}{e^{-K(\lambda)\Lambda}} E_\sigma(\lambda) \tag{13}$$

where $E_\sigma(\lambda)$ is the measured irradiance from the downwards looking spectrometer.

2.6 Geo-registration of reconstructed reflectance profiles

Through the motion of the AUV a series of spectral reflectance measurements along the transect of the AUV survey were produced. The vehicle typically travelled at 0.5m/s and reflectance profiles were reconstructed at 1.5Hz. The centroid location and footprint radius of each measurement were projected onto a mosaic map, reconstructed from the stereo imagery using the relationships estimated of the pose of the AUV and relative terrain positioning from the on-board navigation and mapping systems. These poses were estimated using the information from the pressure sensors, compass, tilt sensors, Ultra-Short Base Line (USBL) positioning system and feature matching of the stereo camera using a Simultaneous Localisation and Mapping (SLAM) algorithm (Williams et al., 2012). The position of the hyperspectral spot can be defined by:

$$p_f^{NED} = p_{AUV}^{NED} + C_c^{NED} p_f^c \tag{14}$$

where p_f^{NED} is the georeferenced coordinate of the hyperspectral spot in an NED (North-East-Down) reference frame, p_{AUV}^{NED} is the position of the AUV in the NED frame, C_c^{NED} is the direction cosine matrix representing the AUV's orientation and p_f^c is the position of the hyperspectral spot measurement in the stereo camera frame of reference (derived using the techniques outlined in Section 2.4).

2.7 Classification of seafloor biota from reconstructed reflectance spectra

A supervised classification scheme was developed that used reconstructed reflectance spectra measured at the seafloor to classify different seafloor organisms and surface types. Pairs of reflectance profiles and associated colour images from the stereo camera were extracted and used by a marine biologist to produce a list of dominant classes of objects present, including seafloor biota and substrate types. A subset of the image data was then labelled by the biologist and the corresponding reflectance spectra used as training data for a classification algorithm. Several supervised classification techniques such as (Support Vector Machine (SVM)), Decision Trees, K-Nearest Neighbours (KNN), Ensemble Boosting and Bagging were used to evaluate variations in performance owing to algorithm selection. The classification algorithms were implemented using the Statistics and Machine Learning Toolbox within Matlab (MATLAB, 2014). The raw values of the recovered reflectance within the range of 400 to 800nm with a resolution of 1nm were used directly as the feature vector.

To compare the relative performance of classification based on reflectance data to imagery data, classifiers were also trained by using stereo image-based texture features and extracted RGB colour data. Local Binary Pattern (LBP) (Ojala et al., 2002) were extracted from the colour stereo imagery corresponding to the disc of seafloor encompassed by the spectrometer's FOV using the calibration relationships discussed in Section 2.4. Two LBPs were computed on the image spot; one LBP had a radius of 1 pixel with surrounding 8 points and the other with a radius of 3 pixels with surrounding 8 points. This combination was chosen based on its success in the literature with classifying underwater imagery from an AUV (Bewley et al., 2015). The histogram of both LBPs were used as the feature vector for classification. Patches of image colour were extracted from the camera images and corrected for water attenuation using Equations 13. Four separate classifiers were developed; one based only on reflectance profiles, one based only on image texture, one based only on RGB data and one based on a combination of reflectance and texture features. For each type of classifier, automatic feature selection was performed while training the classifier to ensure the greatest inter-class variability in the feature matrix (Friedman, 2013). When testing and training, the dataset was whitened by subtracting the mean and dividing by the variance at the feature level.

3 Results

3.1 Experimental setup

Data collected from an AUV survey over a coral shoal at Pakhoi Bank ($+147.883°N$, $-19.441°E$), on the Great Barrier Reef (GBR), Queensland, Australia (17th December 2013, 14:02 - 16:40) was used to demonstrate our methodology. The AUV followed a coarse-grid transect with approximately 100m in-between parallel grid lines. This was a long mission where 14,168 stereo pairs of images and corresponding spectrometer readings were taken over a total path length of approximately 4.5km. The mean depth of operation was 27.1m and mean altitude was 2.2m (AUV from seafloor). This was one of many surveys conducted over small shoals on the Great Barrier Reef (GBR) approximately 40kms off the coast of Townsville, Australia (Roberts et al., 2015). A wide variety of substrates and biota were present in the study region including sandy and rocky bottoms, coral rubble, live coral of several different genera, sea grass and other turf and encrusting species of macro and micro algae.

3.2 Spectral reflectance profiles

Figures (6 to 10) illustrate corresponding pairs of image data (a) and recovered reflectance spectra (b) where the red circle in images indicates the FOV of the spectrometer. Figure 6 (c) and (d) additionally show the measured ambient light irradiance (at the surface and at the depth of the AUV) and the estimated attenuation coefficient ($K(\lambda)$), each as a function of wavelength.

(a) Red-Green-Blue (RGB) image of the coral imaged, red circle is the FOV of the spectrometer

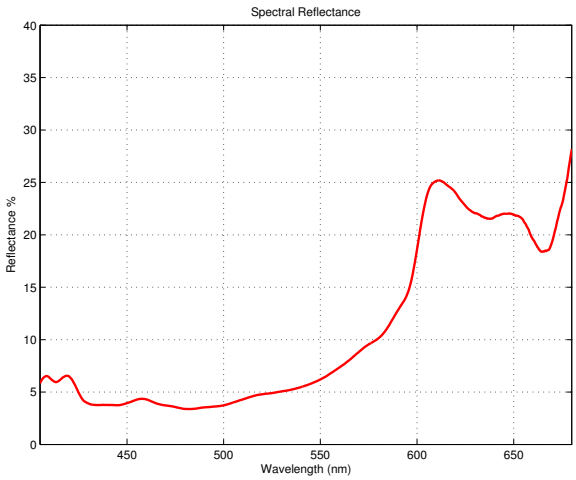

(b) Estimated reflectance of the coral

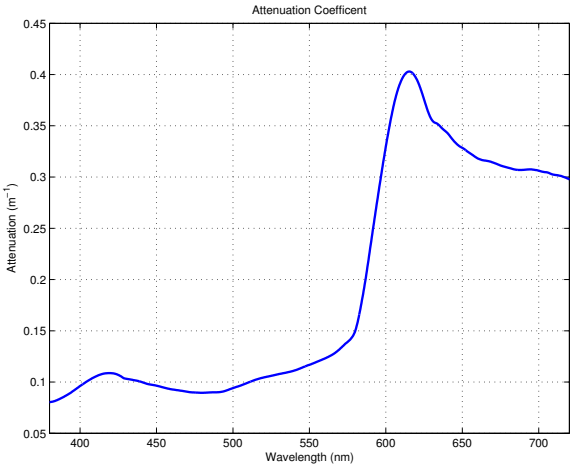

(c) The modelled attenuation coefficient curve based primarily on the upward spectrometer readings

Figure 6: Spectral reflectance of *Acropora sp. 1* coral

By examining the spectral reflectance we are able to extract more information about the pigments that may be present within each seafloor class. The coral species shown in Figure 7 (*Montipora sp.*) exhibits a higher green pigment (475-575nm) than the more distinctly brown colouration of the coral observed in Figure 6 (*Acropora sp. 1*). The distinctive blue tips of the coral *Acropora sp. 2* (Figure 9) are seen as a small peak in the spectral reflectance around 480nm. The seagrass measurement observed in Figure 10 exhibits a distinct chlorophyll absorption (lower reflectance) at 675nm, common for sea grasses and algae. Such differences in absorption and reflectance between biota were important features in the ability to effectively classify biota classes from reflectance signals.

3.3 Mapping results

Figure 11 shows sections of the reconstructed mosaic imagery maps and associated reflectance spot locations, with annotated labels of the corresponding seafloor classes. These maps illustrate single-transect sections (approximately 2m wide) from broad scale transects.

Figure 11a shows a section of the survey mission over a sand to seagrass transition. This section was not

(a) RGB image of the coral imaged, red circle is the FOV of the spectrometer

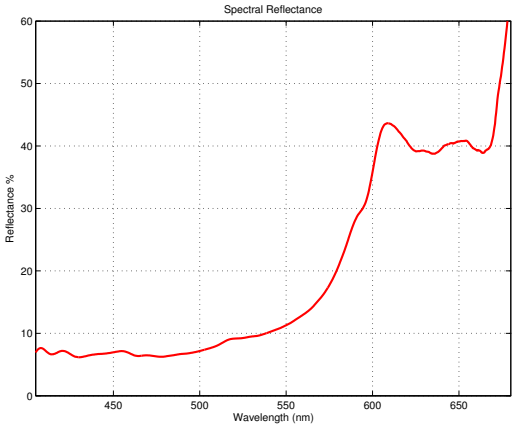

(b) Estimated spectral Reflectance

Figure 7: Spectral reflectance of *Montipora sp.* coral

(a) RGB image

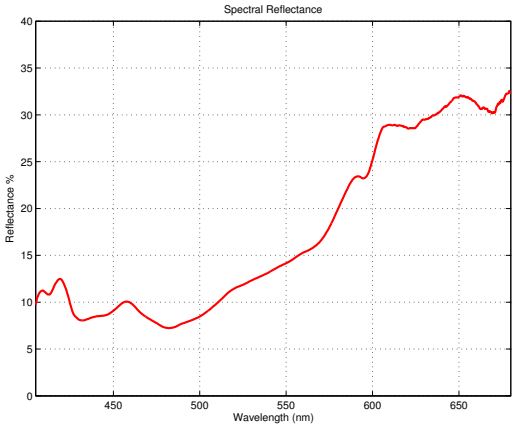

(b) Spectral Reflectance of the sand

Figure 8: Sand reflectance

(a) RGB image

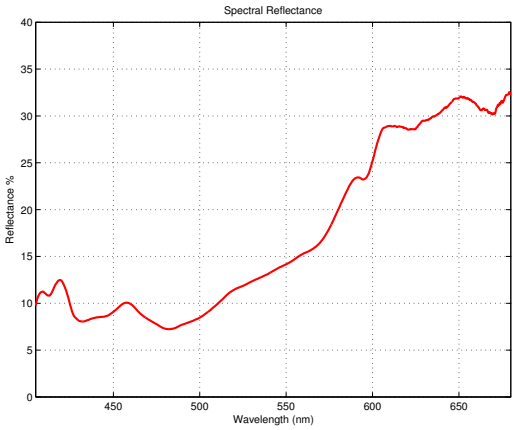

(b) Spectral Reflectance of the sample

Figure 9: *Acropora sp. 2* coral reflectance

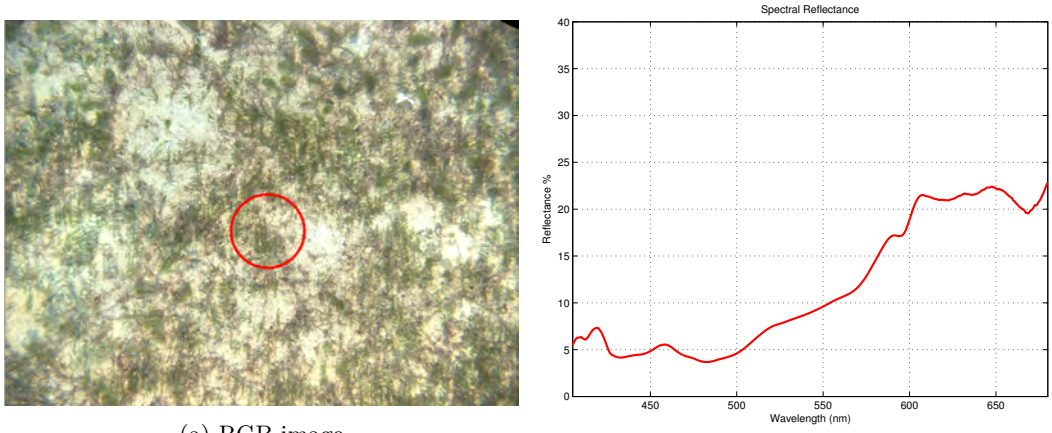

(a) RGB image

(b) Spectral Reflectance

Figure 10: Seagrasses - *Halophila spinulosa* and *Halophila decipiens*

included in the classification training dataset and so demonstrates typical test set classification performance. Major substrates that were present in the data were classified with high accuracy. Some misclassification of coral (Figure 11b) was present due in part to the number of training samples in the model and the size of the material within the FOV of the spectrometer. This aspect is discussed further in the next section. Figure 11c like the previous figure demonstrates the typical classification performance over a section of coral reef.

3.4 Classification performance

Table 1 shows the resulting classification performances (accuracy) for the four different combinations of features employed and different classification algorithms used, evaluated using 10-fold cross validation. It was found that a Linear SVM with a combination of the hyperspectral reflectance and LBP features performed the best with a classification accuracy at 91.99% $\pm$ 2.32. Use of the hyperspectral reflectance profile as a sole feature consistently out-performed the classification based on either image texture of three-channel RGB image colour (excepting marginal differences when using an SVM with radial basis functions).

Use of image texture (LBP) on it's own as a feature vector using the Ensemble Boosting method resulted in a good classified rate of 82.38%. In comparison the HS feature descriptor performed better (91.69%) than a LBP using a Linear SVM. When examining the combined HS + LBP results, the performance increase above HS alone was slight.

Table 2 shows the confusion matrix for the Linear SVM LBP+HS trained classifier (best performer), showing the true class of a data point versus the predicted class. The confusion matrix can explain some reasons for a suboptimal classification: Coral rubble is mostly predicted accurately (84.7%), however it is also predicted to be Algae, *Acropora cf. grandis*, Other Corals and *Acropora sp.*. This is likely due to coral rubble being made up of broken dead corals mostly covered in algae. Seagrass was sometimes misclassified (2.1%) because images of seagrass also contain sand. Turf algae was misclassified as coral and rubble (28%) because turf algae is often present over most underwater surfaces. Soft coral was being misclassified as *Acropora sp.* (39.3%) most likely because the process is picking up on a pigment common to most corals (Hochberg et al., 2006; Hedley and Mumby, 2002) and the small number of samples of soft coral.

There will also be confusion due to the relatively large spatial coverage of the spectrometer's FOV which often covered more than one material. The spectrometer's FOV has a diameter of approximately 30cm when imaging the seafloor from a height of 2m. This spatial attribute can also explain the poor performance in some classes. CCA, turf algae, encrusting coral, soft coral and cyanobacteria performed poorly. A majority of these biota covered very small regions of the FOV of the spectrometer, resulting in spectral mixing. The

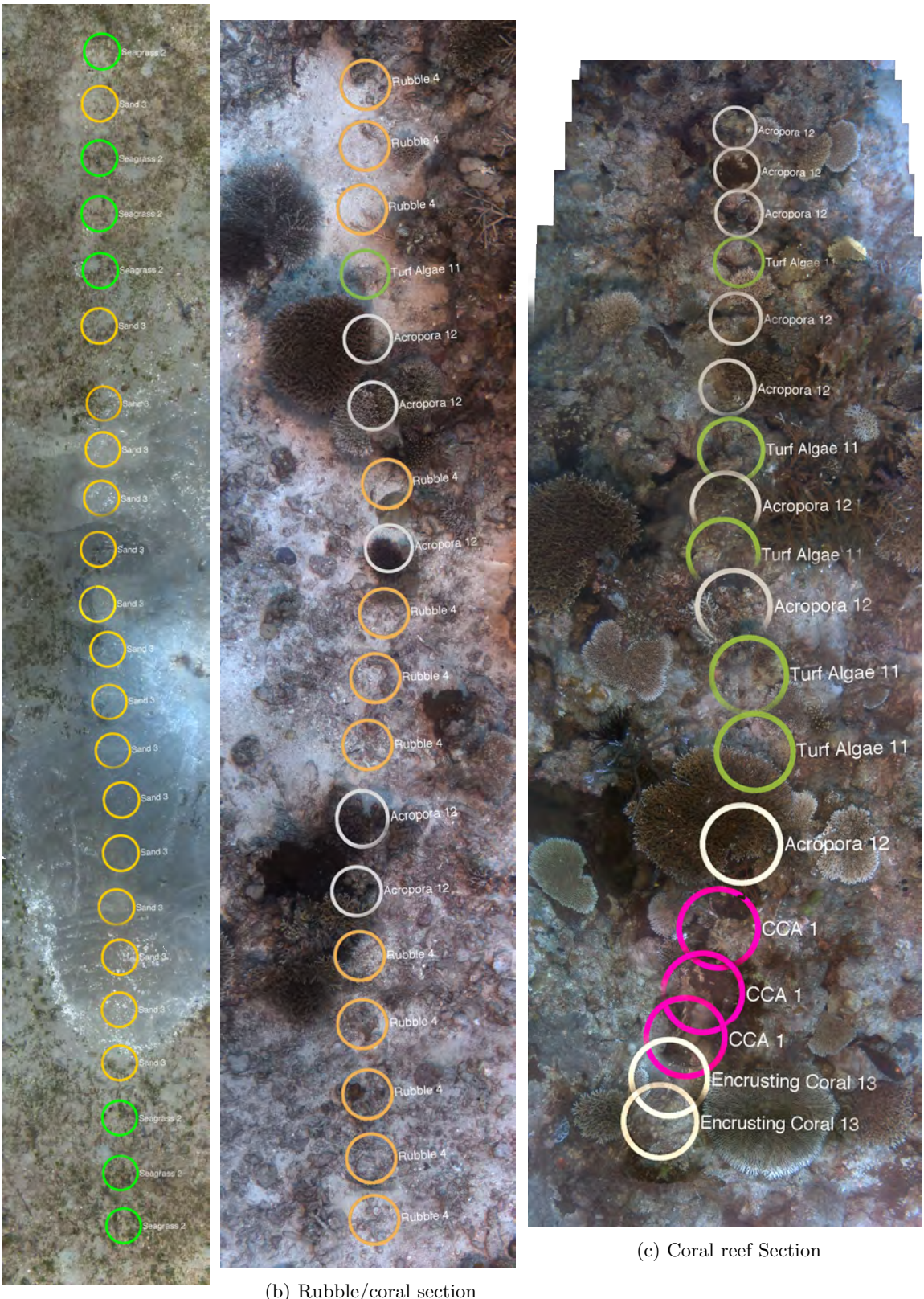

(a) Sand/seagrass

(b) Rubble/coral section

(c) Coral reef Section

Figure 11: (a) Mosaic of a small section of the classification prediction, this shows a transitional section of sand to seagrass. Yellow circles signify a label of Sand, and Green is the label for seagrass. (b) & (c) Mosaics of a small section of the classification prediction, this shows a section of coral reef. They show the transition from sandy substrate to coral and algal substratum.

Classifier	RGB	LBP	HS	HS + LBP
Linear SVM	39.13% ± 0.51%	73.30% ± 1.79%	91.69% ± 1.75%	**91.99% ± 2.32%**
Polynomial SVM	39.13% ± 0.52%	39.13% ± 0.53%	88.41% ± 1.81%	88.48% ± 2.99%
SVM Sigmoid Kernel	39.13% ± 0.46%	39.13% ± 0.41%	71.32% ± 1.67%	71.40% ± 1.77%
SVM Radial Basis Fn	39.13% ± 0.48%	39.66% ± 1.02%	39.13% ± 0.54%	39.13% ± 0.34%
KNN	84.59% ± 1.47%	79.79% ± 3.67%	86.73% ± 1.91%	86.80% ± 1.13%
Ensemble Boosting	82.61% ± 2.07%	82.38% ± 2.42%	91.00% ± 2.28%	89.24% ± 2.56%
Ensemble Bagging	82.68% ± 1.13%	81.08% ± 3.22%	90.92% ± 1.49%	89.40% ± 1.30%
Decision Tree	84.67% ± 2.20%	78.72% ± 2.20%	88.56% ± 2.36%	88.02% ± 2.08%

Table 1: Classification performance (accuracy) for different feature combinations and classification algorithms using 10-fold cross validation on the hand labeled data points (RGB image colour data only, LBP: image texture only, HS: hyperspectral reflectance only and HS+LBP: hyperspectral reflectance and image texture). A linear SVM performed the best on a combination of hyperspectral reflectance data (HS) and LBP. We can see from this table LBP does not contribute much to the performance of the classification over just using HS. Classification results are shown with ± 1 standard deviation.

material they are mixed with will change and thus the spectra for these materials will not be consistent leading to classification errors. To overcome this, either a finer spatial resolution is required or closer measurements of the substrate are needed. For the larger materials such as seagrass, sand, coral rubble and Acropora they all perform well under the 10-fold cross validation due to the reduction in spectral mixing. The limited spatial resolution can be a problem for identifying these smaller materials in the scene.

3.5 Classified seafloor habitat map

Figure 12 shows a 3D map of geo-registered and classified biota data using the best performing classifier described above. From the spatial distribution of classes observed, *Acropora sp.* coral tended to occur around the higher elevation areas on top of the coral outcrops, whereas seagrass was growing in the lower sandy patches. Coral rubble patches were more prevalent on the exposed eastern side of the reef. The prevailing storm and cyclone activity most often came from the south-east of the study region and this was at the edge of a large flat sandy expanse. On the western, inshore, side more live *Acropora sp.* coral was observed.

4 Discussion

4.1 Advantages of our approach

Experimental results shown in our work demonstrate the ability to recover fine-scale hyperspectral reflectance profiles of objects on the seafloor and to use these profiles to accurately classify both biota and substrate types. Our approach allows for the recovery of reflectance data through careful measurement, calibration and mitigation of light in the underwater environment including effects from the water surface and attenuation, accounting for changes in the AUV operating depth and altitude above the underwater terrain. Being able to map biota for example in coral reef habitats at fine resolutions as demonstrated here allows for fine-scale investigations of various indicators of the biological health or productivity of a region and is important in the context of long-term monitoring.

When viewing the seafloor from above the water the light from the sun must pass through the water, reflect off the substrate (sandy substrate 25-35% reflectance, coral 5-10% reflectance) and back through the water column. Our technique allowed us to image at a greater depth and still receive solar illumination, as a result of being in-situ and thus having a shorter optical path length. We also received a stronger reflected signal due to the artificial illumination put out by the AUV.

		Actual class									
		CCA	Seagrass	Sand	Coral Rubble	Turf Algae	Acropora	Encrusting	Sponge	Soft Coral	Cyanobacteria
Predicted class	CCA	**6**	0	0	0	6	0	2	2	2	0
	Seagrass	0	**502**	3	1	0	1	1	0	0	0
	Sand	0	11	**455**	1	0	0	0	0	0	0
	Coral Rubble	0	0	4	**61**	4	0	1	1	4	6
	Turf Algae	4	0	0	5	**15**	3	3	0	0	3
	Acropora	1	0	0	0	4	**130**	4	2	11	0
	Encrusting	2	0	0	0	1	2	**2**	1	1	0
	Sponge	0	0	0	1	0	2	0	**9**	1	0
	Soft Coral	0	0	0	1	0	4	0	0	**9**	0
	Cyanobacteria	0	0	0	2	2	0	0	0	0	**12**
	class size (n)	13	513	462	72	32	142	13	15	28	21
	% correctly predicted	46%	98%	98%	85%	47%	92%	15%	60%	32%	57%

Table 2: Confusion matrix for the classification model using a linear SVM with HSI and LBP data. The model was trained using 10 fold cross-validation on the hand-labelled dataset. CCA - Crustose Coralline Algae, Encrusting - Encrusting Corals. The major classes: Seagrass, Sand, Rubble, Turf Algae and Acropora perform very well, the other smaller classes do not, believed to be in part due to their small numbers to train the classifier. These particular classes were rare in the dataset.

The ability to discriminate seafloor material types at such a fine scale has other applications in the analysis of marine environments. There are several uses for the data in above water applications such as retrieving ground truth spectra for larger scale aerial mapping and collection of the optical properties of a water body for use in correcting remotely sensed data over coastal regions. Often aerial mapping algorithms make large assumptions as to the homogeneity of the water body they are imaging through, whereas our approach continuously estimates and compensates for these parameters during the dive.

4.2 Limitations

The selective absorption of light by water means that data from images or radiometers (i.e. spectrometers) are always limited by the operating distance to the seafloor and to wavelength ranges in which losses are minimised. Light in the near-infrared region of the spectrum (700-900nm) is commonly used as a strong indicator of both species health and for class differentiation in coral, algae and grass species. Our spectrometers received minimal signal in this region due to the heavy absorption by the water. A large amount of light flux would be needed to receive a decent signal in this spectral region. This may not be practical when operating from a battery powered robotic platform.

The second limitation we identified was due in part to the footprint of the spectrometer. The footprint was approximately 30cm in diameter. This altered the degree of material purity in each reading. This influenced the classification performance, the less pure the sample the poorer the performance. This attribute is known as spectral mixing and there are methods for unmixing these combinations of material types, however this is outside of the scope of this work.

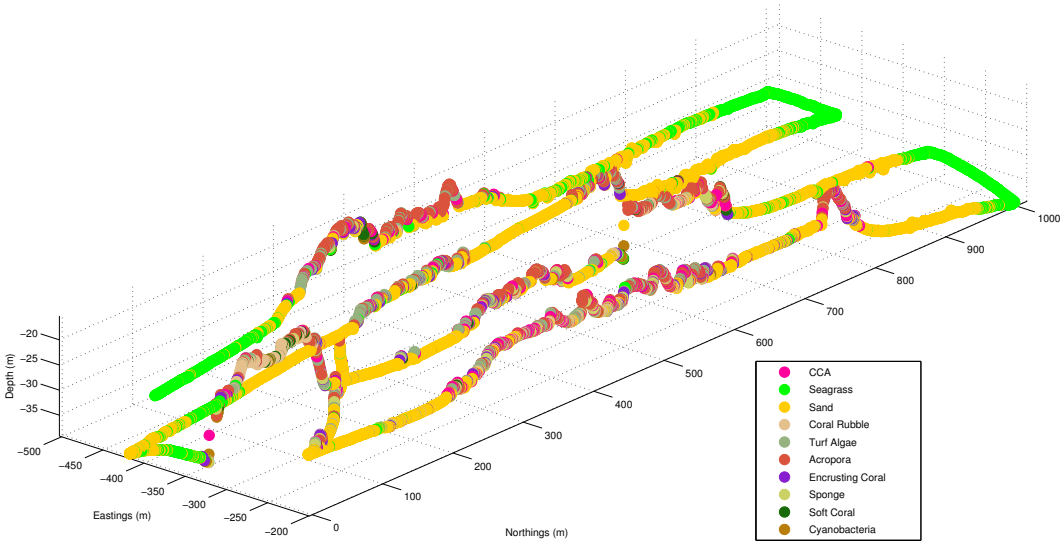

Figure 12: Spectral map from an isometric angle showing the different elevations of the seafloor types. The elevation has been amplified by a factor of 5 to demonstrate the class distribution as a function of elevation further. The key for the class labels is on the right. This dataset contains over 14,000 points, due to the limit of displaying the classified points in this diagram, the entire detail of classification can not be fully shown in this figure. More detailed figures of subsets of the map overlaid on the corresponding image mosaics are shown in Figure 11.

5 Conclusion and Future Work

Above water hyperspectral imaging of the ocean floor (using Remote Sensing) presents many challenges, including limited spatial resolution, air-water interface artefacts, weather reliance, time of day dependence, and depth limitation due to the attenuation of the water column. The ability to reconstruct hyperspectral reflectance information from within the water largely overcomes these limitations. An AUV is an ideal platform for this application, being able to travel to depths beyond the euphotic zone, operations not heavily dependent on surface weather and achieves excellent spatial resolution. Our use of a spectrometer (in contrast to a hyperspectral imager) allowed us to maintain good signal-to-noise ratios while still providing spatial resolutions sufficient for organism classification at a fraction of the size, power, onboard storage/processing power and cost requirements that would be required from an underwater hyperspectral imager.

Future work will examine methods to help resolve sub-footprint abundances of small or rare organisms observed by our system. Processing techniques in the remote sensing literature known as spectral unmixing (Keshava and Mustard, 2002) allow for resolving the fractional abundances of sub-pixel constituents (end-members) by relying on a pre-existing spectral library (Bioucas-dias et al., 2012; Keshava and Mustard,

2002). The high spatial resolution imagery from the stereo cameras on the AUV could also be utilised to assist in resolving the pure end-members for an unsupervised creation of a spectral library of pure end-members (Zortea and Plaza, 2009). Through an inversion processing step, different materials present and their abundances within each footprint could then potentially be resolved.

We used LBP as a feature descriptor for the camera imagery, however other techniques could be incorporated to add more features to our classifier. The 3D data could be used for assisting in coral taxa classification, above water hyperspectral coral classification methods have been unable to distinguish coral on the species level (Hochberg and Atkinson, 2003). An additional classification feature could be the use of rugosity, this has also been shown to be an ecological indicator of bio-productivity (Friedman et al., 2012).

Future work could also consider the use this technique for deriving the health of the coral (Holden and LeDrew, 2001) affected by bleaching or invasive algal blooms. Our methods potentially allows for revisiting large areas of reef to examine the small level changes which may occur over time.

Acknowledgments

The author would like to thank the Australian Institute of Marine Science, the crew of the RV Cape Ferguson and Christian Lees and Andrew Durrant for their excellent support in collecting the field data, Roy Hughes and DSTO for their guidance and assistance. The authors acknowledge support from Australia's Integrated Marine Observing (IMOS) program. IMOS is an initiative of the Australian Government being conducted as part of the National Collaborative Research Infrastructure Strategy (NCRIS). The AUV facility is one of the eleven IMOS facilities funded by NCRIS and provides support for the deployment of AUV systems at benthic reference sites around Australia. The authors also acknowledge the support of the Australian Centre for Field Robotics and the University of Sydney.

Additional online resources

During the AUV operations a GoPro was recording footage from onboard the vehicle, some clips of the region mapped in this paper are shown in the video. The video also shows the water conditions, clarity and light levels. This video may be view at: `http://vimeo.com/84354609`

References

Andréfouët, S., Berkelmans, R., Odriozola, L., Done, T., Oliver, J., and Müller-Karger, F. (2002). Choosing the appropriate spatial resolution for monitoring coral bleaching events using remote sensing. *Coral Reefs*, Volume 21(Number 2):147–154.

Beijbom, O., Edmunds, P. J., Kline, D. I., Mitchell, B. G., and Kriegman, D. (2012). Automated Annotation of Coral Reef Survey Images. In *Computer Vision and Pattern Recognition 2012*, pages 1170–1177.

Bewley, M. S., Nourani-Vatani, N., Rao, D., Douillard, B., Pizarro, O., and Williams, S. B. (2015). Hierarchical Classification in AUV Imagery. In *Field and Service Robotics*, pages 3–16. Springer.

Bioucas-dias, J. M., Plaza, A., Dobigeon, N., Parente, M., Du, Q., Gader, P., and Chanussot, J. (2012). Hyperspectral Unmixing Overview : Geometrical , Statistical , and Sparse Regression-Based Approaches. *Selected Topics in Applied Earth Observations and Remote Sensing, IEEE Journal of*, 5(2):354–379.

Bongiorno, D. L., Bryson, M., Dansereau, D. G., Williams, S. B., and Pizarro, O. (2013a). Spectral Characterisation of COTS RGB Cameras Using a Linear Variable Edge Filter. In *IS&T/SPIE Electronic Imaging*. International Society for Optics and Photonics.

Bongiorno, D. L., Fairley, A. J., Bryson, M., and Williams, S. B. (2013b). Automatic Spectrometer/RGB Camera Spatial Calibration. In *Proceedings of the IEEE International Geoscience and Remote Sensing Symposium*, Melbourne, Australia. IEEE.

Bryson, M., Johnson-Roberson, M., Pizarro, O., and Williams, S. B. (2015). True Color Correction of Autonomous Underwater Vehicle Imagery. *Journal of Field Robotics*, 22(1).

Campos, R., Garcia, R., Alliez, P., and Yvinec, M. (2015). A surface reconstruction method for in-detail underwater 3D optical mapping. *The International Journal of Robotics Research*, 34(1):64–89.

Clement, R., Dunbabin, M., and Wyeth, G. (2005). Toward robust image detection of crown-of-thorns starfish for autonomous population monitoring. In *Australasian Conference on Robotics and Automation 2005*. Australian Robotics and Automation Association Inc.

English, D. C. and Carder, K. L. (2006). Determining Bottom Reflectance and Water Optical Properties Using Unmanned Underwater Vehicles under Clear or Cloudy Skies. *Journal of Atmospheric and Oceanic Technology*, 23(2):314–324.

Friedman, A., Pizarro, O., Williams, S. B., and Johnson-Roberson, M. (2012). Multi-scale measures of rugosity, slope and aspect from benthic stereo image reconstructions. *PloS one*, 7(12):e50440.

Friedman, A., Steinberg, D., Pizarro, O., and Williams, S. B. (2011). Active learning using a Variational Dirichlet Process model for pre-clustering and classification of underwater stereo imagery. In *Intelligent Robots and Systems*, pages 1533–1539.

Friedman, A. L. (2013). *Automated interpretation of benthic stereo imagery*. PhD thesis, University of Sydney.

Guild, L., Lobitz, B., Armstrong, R., Gilbes, F., Gleason, A., Goodman, J., and Hochberg, E. (2003). NASA Airborne AVIRIS and DCS Remote Sensing of Coral Reefs. *Sensing And Imaging*.

Hartmann, K., de Souza, P., Timms, G., Davie, A., and Ieee (2009). Measuring light attenuation with a compact Optical Emission Spectrometer and CTD mounted on a low cost AUV. In *Oceans 2009 - Europe, Vols 1 and 2*, pages 540–544. Ieee, New York.

Hedley, J. D. and Mumby, P. J. (2002). *Biological and remote sensing perspectives of pigmentation in coral reef organisms.*, volume 43.

Hochberg, E. J., Apprill, A., Atkinson, M., and Bidigare, R. (2006). Bio-optical modeling of photosynthetic pigments in corals. *Coral Reefs*, 25(1):99–109.

Hochberg, E. J. and Atkinson, M. J. (2003). Capabilities of remote sensors to classify coral, algae, and sand as pure and mixed spectra. *Remote Sensing of Environment*, 85(2):174–189.

Hoegh-Guldberg, O., Mumby, P. J., Hooten, a. J., Steneck, R. S., Greenfield, P., Gomez, E., Harvell, C. D., Sale, P. F., Edwards, a. J., Caldeira, K., Knowlton, N., Eakin, C. M., Iglesias-Prieto, R., Muthiga, N., Bradbury, R. H., Dubi, a., and Hatziolos, M. E. (2007). Coral reefs under rapid climate change and ocean acidification. *Science (New York, N.Y.)*, 318(5857):1737–42.

Holden, H. and LeDrew, E. (2001). Hyperspectral Discrimination of Healthy versus Stressed Corals Using in Situ Reflectance. *Journal of Coastal Research*, 17(4):850–858.

Idris, M., Jean, K., and Zakariya, R. (2009). Hyperspectral Discrimination and Separability Analysis of Coral Reef Communities in Redang Island. *Journal of Sustainability Science and Management*, 4(2):36–43.

Johnsen, G., Volent, Z., Dierssen, H., Pettersen, R., Van Ardelan, M., Søreide, F., Fearns, P., Ludvigsen, M., and Moline, M. (2013). Underwater hyperspectral imagery to create biogeochemical maps of seafloor properties. In *Subsea optics and imaging*, pages 508–535. Woodhead Publishing Limited.

Keshava, N. and Mustard, J. F. (2002). Spectral Unmixing. *IEEE Signal Processing Magazine*, (January).

Kobryn, H. T., Wouters, K., Beckley, L. E., and Heege, T. (2013). Ningaloo Reef: Shallow Marine Habitats Mapped Using a Hyperspectral Sensor. *PLoS ONE*, 8(7):e70105.

Koepke, P. (1984). Effective reflectance of oceanic whitecaps. *Applied optics*, 23(11):1816.

MATLAB (2014). *version R2014b*. The MathWorks Inc., Natick, Massachusetts, USA.

Mehta, A., Ribeiro, E., Gilner, J., and van Woesik, R. (2007). Coral reef texture classification using support vector machines. In *VISAPP (2)*, pages 302–310.

Mishra, D. R., Narumalani, S., Rundquist, D., Lawson, M., and Perk, R. (2007). Enhancing the detection and classification of coral reef and associated benthic habitats: A hyperspectral remote sensing approach. *Journal of Geophysical Research*, 112(C08014).

Mobley, C. D. (1994). *Light and water: Radiative transfer in natural waters*, volume 592. Academic Press.

Ojala, T., Pietikäinen, M., and Mäenpää, T. (2002). Multiresolution Gray-Scale and Rotation Invariant Texture Classification with Local Binary Patterns. *IEEE Transactions on Pattern Analysis and Machine Intelligence*, 24(7):971–987.

Pizarro, O., Rigby, P., Johnson-Roberson, M., Williams, S. B., and Colquhoun, J. (2008). Towards image-based marine habitat classification. *Oceans 2008*.

Quan, X. and Fry, E. S. (1995). Empirical equation for the index of refraction of seawater. *Applied optics*, 34(18):3477–80.

Roberts, T. E., Moloney, J. M., Sweatman, H. P. a., and Bridge, T. C. L. (2015). Benthic community composition on submerged reefs in the central Great Barrier Reef. *Coral Reefs*, 34(2):569–580.

Roelfsema, C. M. and Phinn, S. R. (2012). Spectral reflectance library of selected biotic and abiotic coral reef features in Heron Reef. Technical report, Centre for Remote Sensing & Spatial Information Science, School of Geography, Planning & Environmental Management, University of Queensland, Brisbane, Australia.

Savitzky, A. and Golay, M. J. E. (1964). Smoothing and Differentiation of Data by Simplified Least Squares Procedures. *Analytical Chemistry*, 36(8):1627–1639.

Singh, H., Armstrong, R., Gilbes, F., Eustice, R., Roman, C., Pizarro, O., and Torres, J. (2004). Imaging Coral I : Imaging Coral Habitats with the SeaBED AUV. *Subsurface Sensing Technologies and Applications*, 5(1):25–42.

Spillane, M. C., Monahan, E. C., Bowyer, P. A., Doyle, D. M., and Stabeno, P. J. (1986). Whitecaps and Global Fluxes. In Monahan, E. and Niocaill, G., editors, *Oceanic Whitecaps SE - 19*, volume 2 of *Oceanographic Sciences Library*, pages 209–218. Springer Netherlands.

Torres-Mendez, L. A. and Dudek, G. (2005). A Statistical Learning-Based Method for Color Correction of Underwater Images. In *Research on Computer Science Vol. 17, Advances in Artificial Intelligence Theory*.

Vasilescu, I., Detweiler, C., and Rus, D. (2010). Color-Accurate Underwater Imaging using Perceptual Adaptive Illumination. In *Robotics: Science and Systems*.

Volent, Z., Johnsen, G., and Sigernes, F. (2007). Kelp forest mapping by use of airborne hyperspectral imager. *Journal of Applied Remote Sensing*, 1.

Wang, K., Franklin, S. E., Guo, X., and Cattet, M. (2010). Remote sensing of ecology, biodiversity and conservation: a review from the perspective of remote sensing specialists. *Sensors (Basel, Switzerland)*, 10(11):9647–67.

Wilkinson, C. (2008). *Status of coral reefs of the world: 2008*. Global Coral Reef Monitoring Network.

Williams, S., Pizarro, O., Jakuba, M., Johnson, C., Barrett, N., Babcock, R., Kendrick, G., Steinberg, P., Heyward, A., Doherty, P., Mahon, I., Johnson-Roberson, M., Steinberg, D., and Friedman, A. (2012). Monitoring of Benthic Reference Sites: Using an Autonomous Underwater Vehicle. *Robotics and Automation Magazine, IEEE*, 19(1):73 – 84.

Williams, S. B., Pizarro, O., Webster, J. M., Beaman, R. J., Mahon, I., Johnson-Roberson, M., and Bridge, T. C. L. (2010). Autonomous Underwater Vehicle-Assisted Surveying of Drowned Reefs on the Shelf Edge of the Great Barrier Reef, Australia. *Journal of Field Robotics*, 27(5):675–697.

Zortea, M. and Plaza, A. (2009). Spatial preprocessing for endmember extraction. *Geoscience and Remote Sensing, IEEE Transactions on*, 47(8):2679–2693.